JGR Oceans

RESEARCH ARTICLE
10.1029/2020JC016080

Key Points:
- Impact of transmission scheme of visible solar radiation (VSR) on temperature and mixing in the upper ocean is investigated
- The required input (chlorophyll or inherent optical properties) for the scheme is derived from the same ocean color remote sensing
- Different VSR transmission schemes can lead to significant differences in vertical temperature profile, although all use the same color data

Correspondence to:
T. Liu and Z. Lee,
zhongping.lee@umb.edu;
liutongtong@stu.xmu.edu.cn

Citation:
Liu, T., Lee, Z., Shang, S., Xiu, P., Chai, F., & Jiang, M. (2020). Impact of transmission scheme of visible solar radiation on temperature and mixing in the upper water column with inputs for transmission derived from ocean color remote sensing. *Journal of Geophysical Research: Oceans*, *125*, e2020JC016080. https://doi.org/10.1029/2020JC016080

Received 16 JAN 2020
Accepted 27 MAY 2020
Accepted article online 29 MAY 2020

Impact of Transmission Scheme of Visible Solar Radiation on Temperature and Mixing in the Upper Water Column With Inputs for Transmission Derived From Ocean Color Remote Sensing

Tongtong Liu[1], Zhongping Lee[2], Shaoping Shang[1], Peng Xiu[3], Fei Chai[4,5], and Mingshun Jiang[6]

[1]College of Ocean and Earth Sciences, Xiamen University, Xiamen, China, [2]School for the Environment, University of Massachusetts Boston, Boston, MA, USA, [3]State Key Laboratory of Tropical Oceanography, South China Sea Institute of Oceanology, Chinese Academy of Sciences, Guangzhou, China, [4]School of Marine Sciences, University of Maine, Orono, ME, USA, [5]State Key Laboratory of Satellite Ocean Environment Dynamics, Second Institute of Oceanography, Hangzhou, China, [6]Harbor Branch Oceanographic Institute, Florida Atlantic University, Fort Pierce, FL, USA

Abstract The penetration of visible solar radiation (VSR) in the upper ocean contributes to heating in the upper water column, and this process is modulated by constituents in water such as phytoplankton. Various schemes have been developed to propagate surface VSR to deeper depths, which are incorporated in ocean circulation models to study basin-scale impacts on ocean and atmosphere by phytoplankton. However, none of these studies evaluated sensitivity of the schemes of VSR transmission to upper-water dynamics, especially when the required input is derived from ocean color remote sensing. We used an idealized one-dimensional (1-D) Regional Ocean Modeling System (ROMS) to simulate profiles of upper water column temperature at six locations with different ocean color characteristics (containing different water constituents). We incorporated and tested four different schemes of VSR transmission: the default water-type scheme within the ROMS, two schemes based on concentrations of chlorophyll (Chl), and one scheme based on water's inherent optical properties (IOPs). The results showed that, although using the same ocean color information and the same circulation model, the IOPs- and Chl-based schemes resulted in very different vertical temperature and upper-water mixing compared to those using the default scheme, with differences in sea surface temperature up to 1.5–2°C. These results highlight the importance of developing and incorporating more appropriate VSR transmission schemes into large-scale ocean circulation simulations, where the inputs for the transmission are inherently estimates from ocean color—the actual measurement from satellite remote sensing.

Plain Language Summary Solar irradiance is the most important energy source for the Earth. In the past decades, many transmission schemes were developed to quantify the penetration of visible solar radiation (VSR) in the upper ocean, which were incorporated into general circulation models to evaluate the effects of VSR on upper-ocean and atmospheric dynamics. In this work, we incorporate four different transmission schemes (one based on water type; one based on inherent optical properties, or IOPs based; and two based on chlorophyll concentration, or Chl based) in a one-dimensional ocean general circulation model. We found that, although all transmission schemes used the same data from ocean color remote sensing—the source to derive the required input for the transmission schemes, the IOPs- and Chl-based schemes resulted in very different vertical temperature and upper-water mixing, which were also different from those based on water type. Because the VSR profiles estimated based on IOPs are more accurate for oceanic and coastal waters, these results advocate the application of IOPs products from ocean color satellite to study upper-ocean dynamics in the global oceans and related air-sea interactions.

1. Introduction

Solar irradiance is the most important energy source for the Earth. It determines weather and climate of the Earth system and drives photosynthesis to produce food on land and in the ocean. Because visible solar radiation (VSR, usually ~400 to 700 nm) can penetrate into the upper ocean, it also modulates

Table 1
Terms and Definitions

Symbol	Definition	Units
a	Absorption coefficient	m^{-1}
A_i	O00 coefficients for solar transmission parameterizations	—
b_b	Backscattering coefficient	m^{-1}
B_{1-4}	O00 linear regression coefficients for estimation of A_i	—
C_{1-4}	O00 linear regression coefficients for estimation of K_i	—
Chl	Chlorophyll a concentration	mg m^{-3}
C_p	Specific heat of seawater	J (kg °C)$^{-1}$
E	Downwelling irradiance measured in water	W m^{-2}
F_{IR}	M02 partitioning factor for infrared domain	Dimensionless
F_{VIS}	M02 partitioning factor for visible domain	Dimensionless
K_1 , K_2	L05 contributors for the attenuation coefficient at greater depths and subsurface, respectively	m^{-1}
K_i	O00 exponents for solar transmission parameterizations	m^{-1}
K_{IR}	Attenuation coefficient for infrared domain	m^{-1}
K_{SR}	Attenuation coefficient of solar radiation	m^{-1}
K_{VIS}	Attenuation coefficient for visible domain	m^{-1}
R	PS77 partitioning factor for visible domain	Dimensionless
RHR	Ocean radiant heating rate	°C s^{-1}
Rrs	Remote sensing reflectance	sr^{-1}
V_{1-2}	M02 partitioning factors	Dimensionless
T	Temperature of sea water	°C
Tr	Transmittance of downwelling irradiance	Dimensionless
Tr_{IR}	Transmittance in the infrared domain	Dimensionless
Tr_{VIS}	Transmittance in the visible domain	Dimensionless
z	Depth	m
θ_a	Solar zenith angle above surface	deg
θ_w	Solar zenith angle below surface	deg
ξ_{1-2}	PS77 e-folding depths of the near-infrared and visible domain of solar radiation	m
ρ_w	Density of sea water	kg m^{-3}
ζ_{0-2} ,α_{0-2},χ_{0-2}	L05 parameters for K_{VIS}	Dimensionless

upper-ocean temperature and mixing patterns (Lewis et al., 1990; Zaneveld et al., 1981). Therefore, the inclusion of solar flux, especially the vertical distribution of VSR in ocean circulation or ecosystem models, is important for modeling heating, mixing, circulation, and biological responses.

The heating influence of solar radiation on an upper-ocean layer with a thickness of Δz (m) can be represented by ocean radiant heating rate (RHR), which is commonly described by

$$\mathrm{RHR}(z) = \frac{\Delta T}{\Delta t} = \frac{E(z1) - E(z2)}{\rho_w C_p \Delta z}, \tag{1}$$

where T is ocean temperature; t is time; $E(z1)$ and $E(z2)$ are the total downwelling irradiance (E) at depths $z1$ (m) and $z2$, respectively; and $\Delta z = z2 - z1$. ρ_w is seawater density, and C_p is the specific heat of sea water (Zaneveld et al., 1981). A list of variables used in this paper is presented in Table 1.

Total downwelling irradiance at surface ($E(0)$) can be determined using the Sun's position and atmospheric properties (Frouin et al., 1989). The irradiation at any depth z, $E(z)$, is calculated from $E(0)$ and the transmittance (Tr) between surface and z:

$$E(z) = Tr(z) \times E(0). \tag{2}$$

In most dynamic ocean models (e.g., Regional Ocean Modeling System, ROMS), solar radiation reaching a water layer is calculated following Equation 2, with $E(0)$ as forcing condition or from a light model (Hedström, 2000), while $Tr(z)$ is calculated following a scheme (see a few examples in section 2.1). Since $E(0)$ is generally the same for various dynamic models, the accuracy of Tr scheme will affect the estimate of $E(z)$ and, subsequently, the heating rate and upper-ocean dynamics.

E includes energy from the ultraviolet (UV) to shortwave wavelengths. For efficient calculation in a dynamic ocean model, *E* is usually divided into two parts (Morel & Antoine, 1994): the energy of infrared-shortwave domain with wavelength > ~700 nm, and the other part for VSR. Because the proportion of solar radiation in the UV wavelength is small (Mecherikunnel & Richmond, 1980) and rapidly absorbed near the water surface (Mobley, 1994), UV contribution in a dynamic ocean model is either ignored or implicitly included in the "visible" term. Solar radiation in the infrared-shortwave domain is quickly absorbed by waters near the surface (< ~1–2 m), and it is the vertical penetration of VSR that contributes to heating the waters below the surface layer (e.g., Morel & Antoine, 1994). Therefore, an accurate estimate of the vertical distribution of VSR in the upper water column is important for representing this heating process, which has been a research topic in the past decades (e.g., Lee et al., 2005; Morel & Antoine, 1994; Ohlmann & Siegel, 2000).

Historically, and even today, the most widely used scheme for *Tr* in a dynamic ocean model (e.g., ROMS) is that of Paulson and Simpson (1977), which is a sum of two exponential terms used to describe the attenuation of solar radiation, with the attenuation coefficients determined based on Jerlov water types (Jerlov, 1968). In the earlier days, the determination of a water type was quite arbitrary. With the availability of chlorophyll concentration (Chl; mg m^{-3}) from ocean color satellite, a scheme to determine water type based on Chl has been developed (Morel, 1988). However, because of the limited number of Jerlov water types, a wide range of Chl can be classified into the same water type; thus, large errors will be introduced in the estimated transmission of solar radiation. More precise and objective methods are desired. Since Chl map of the global ocean is available, various schemes were developed in the past decades to estimate the transmission of VSR using Chl directly (e.g., Morel, 1988; Morel & Antoine, 1994; Ohlmann & Siegel, 2000). Subsequently, many studies employed satellite Chl products in ocean circulation models to evaluate the impact of Chl on upper-ocean dynamics and on heat exchange between ocean and atmosphere. For instance, using the Chl data from the Coastal Zone Color Scanner (CZCS), Nakamoto et al. (2001) compared the results of Paulson's equation and Chl-based scheme of Morel and Antoine (1994) and found that sea surface temperature (SST) would decrease by up to 2°C and mixed layer depth (MLD) would change by 20 m when using Chl instead of using a water-type scheme. Also, Murtugudde et al. (2002) found that a simple exponential equation for the transmission of VSR would improve climate model simulations, when incorporating Chl information. Furthermore, studies (e.g., Jolliff et al., 2012; Lin et al., 2007; Shell et al., 2003; Zhang et al., 2011) showed that considering Chl would not only affect SST but also dynamic processes and air-sea exchange. In short, these efforts showed the advantages and improvements when using Chl, rather than water type, to derive *Tr*. In these studies, however, the accuracy of *Tr* based on remotely estimated Chl was not considered.

It is well known, however, that the attenuation of solar radiation, an optical property of any aquatic environment, is not governed by Chl alone (Sathyendranath et al., 1989). The colored dissolved organic matter (CDOM) also modifies the transmission of VSR, subsequently affecting upper-ocean mixing (Fujii et al., 2007). Also, there are several Chl-based *Tr* schemes (in Equation 2), but it is not clear which one is more suitable for basin-scale circulation applications. This is because the accuracy of Chl-based *Tr* profiles is determined by a combination of two components: accuracy of the *Tr* scheme and accuracy of remotely sensed Chl. To compare the performances of these *Tr* schemes, Zoffoli et al. (2017) showed that the *Tr* profiles estimated based on remotely sensed Chl have a wide range of uncertainties compared to in situ measurements. Lee et al. (2005) developed a *Tr* scheme as a function of the total absorption and backscattering coefficients, properties that could also be derived from ocean color remote sensing. For the same ocean color measurements, Zoffoli et al. (2017) showed that the estimated *Tr* profiles based on remotely estimated inherent optical properties (IOPs) are much more consistent with those of in situ measurements in both oceanic and coastal waters. Compared to Chl, IOPs are more suitable for simulating *Tr* because optical properties of natural waters are indeed determined not only by Chl but also by CDOM and suspended sediments (Sathyendranath et al., 1989).

Recently, Shulman et al. (2017) suggested that in a dynamic ocean model there are three error sources related to solar radiation at depth: (1) errors in $E(0)$, (2) errors in the attenuation (transmission) scheme, and (3) errors in the attenuation coefficient. They pointed out that coupled errors between $E(0)$ and attenuation coefficient can significantly affect the modeled heat exchange when using the scheme of Paulson and Simpson (1977). Mobley et al. (2015) showed that Chl concentration from biogeochemical simulations,

Table 2
Coefficients of the PS77 Scheme for Different Water Types

Water type	Chl (mg m^{-3})	R	ξ_1 (m)	ξ_2 (m)
I	0–0.01	0.58	0.35	23
IA	0.05	0.62	0.6	20
IB	0.1	0.67	1	17
II	0.5	0.77	1.5	14
III	1.5–2.0	0.78	1.4	7.9

where light at depth plays an important role, is 57% higher when accurate irradiance is used compared to that based on a simple exponential attenuation formula. However, Shulman et al. (2017) did not evaluate the impact of the second error source (schemes used to model *Tr*). It is thus important and necessary to evaluate the impact of the *Tr* scheme on the upper-ocean dynamics. This is even more important for basin-scale modeling of ocean circulations, where the sole available source related to *Tr* is the measurement of ocean color (IOCCG, 2020), while Chl or IOPs data are derived products from such measurements, and Chl product has higher uncertainties than IOPs product (Lee et al., 2010).

In this study, we employed the one-dimensional (1-D) ROMS to simulate temperature profiles of six locations with different water properties, in order to understand the combined impact of *Tr* scheme and remote sensing products on heating up the upper ocean. We compared the resulting temperature and MLD from four different *Tr* schemes that use water type, Chl, or IOPs as input. Note that both Chl and IOPs are derived from the same remote sensing reflectance, that is, they are the same input. Similar to earlier numerical studies (Jolliff et al., 2012; Sweeney et al., 2005) and consistent with the default Paulson and Simpson (1977) scheme in the ROMS, we assumed all IOPs to be vertically constant. The remainder of the paper is organized as follows. In section 2, we briefly describe the four different transmission schemes and the idealized 1-D model. In section 3, we present the results of temperature and MLD from the ROMS simulations. In section 4, we discuss the implications of these results, followed by conclusions in section 5.

2. Methods

2.1. Light Transmission Schemes Evaluated

We evaluated four light transmission schemes to characterize the combined impact of transmission scheme and remote sensing product on upper-ocean dynamics. These schemes include Paulson and Simpson (1977) (PS77), Ohlmann and Siegel (2000) (O00), Murtugudde et al. (2002) (M02), and Lee et al. (2005) (L05). It is worth noting that the wavelength ranges of these four schemes are different. The wavelength range of PS77 is 400–1,000 nm, while that of M02 is 380–700 nm. They are 250–2,500 and 350–2,500 nm for O00 and L05, respectively. Because the shortwave radiation in the ROMS is from 300 to 4,000 nm, and the solar radiation in the 300–400 nm and 2,500–4,000 nm ranges contributes <1% of the total irradiance, we applied the *Tr* equations of O00 and L05 without any modifications. However, we adjusted the formulae of PS77 and M02 to match the wavelength range of the forcing condition as described below.

2.1.1. PS77 Scheme

The PS77 scheme is the default in the ROMS, where transmittance of light intensity is modeled as a sum of two exponential functions that represent the attenuation in the near-infrared and visible domains of solar radiation.

$$Tr_{PS77}(z) = Re^{-\left(z/\xi_1\right)} + (1-R)e^{-\left(z/\xi_2\right)} \tag{3}$$

where z is depth positively downward from the surface, R represents the fraction of total solar radiation in the visible domain, and ξ_1 and ξ_2 are the e-folding depths of the two terms with values dependent on Jerlov water types. Table 2 lists the values of R, ξ_1, and ξ_2 for water types encountered in this study.

Because the wavelength range of PS77 is from 400 to 1,000 nm but the shortwave radiation is from 300 to 4,000 nm, and because the irradiance of 1,000–2,500 nm contributes about 24% of the shortwave irradiance in the ~300–2,500 nm range based on simulations of solar radiation (Ricchiazzi et al., 1998), we adjusted Equation 3 to

$$Tr_{PS77}(z) = 0.76\left[Re^{-\left(z/\xi_1\right)} + (1-R)e^{-\left(z/\xi_2\right)}\right] + 0.24\, e^{-(120^*z)} \tag{4}$$

The value 120.0 m^{-1} in the second term on the right-hand side of Equation 4 is an estimated attenuation coefficient for solar radiation of wavelengths 1,000–2,500 nm based on water's absorption coefficient (Kou et al., 1993). This high value shows that solar radiation in this wavelength range is lost in the upper few centimeters.

Morel (1988) developed empirical relationships between Chl and water types (see Table 2). Thus, for a given Chl from ocean color remote sensing, values of ξ_1 and ξ_2 can be adequately determined and implemented in Equation 4.

2.1.2. O00 Scheme

The transmission scheme of Ohlmann and Siegel (2000) is more complex than the other Chl-based schemes (Morel, 1988; Morel & Antoine, 1994). *Tr* in O00 is expressed as a sum of four exponential functions,

$$Tr_{O00}(\mathrm{Chl}, z, \theta_\alpha) = \sum_{i=1}^{4} A_i e^{-K_i z} \tag{5}$$

with A_i and K_i modeled as functions of Chl:

$$A_i = B_{1,i}\mathrm{Chl} + B_{3,i}(\cos(\theta_\alpha))^{-1} + B_{4,i} \tag{6a}$$

$$K_i = C_{1,i}\mathrm{Chl} + C_{3,i}(\cos(\theta_\alpha))^{-1} + C_{4,i} \tag{6b}$$

Here, θ_α is the above-surface solar zenith angle; $B_{1-4,i}$ and $C_{1-4,i}$ are model coefficients that were determined empirically from numerical simulations (Ohlmann & Siegel, 2000). In addition, O00 transmision scheme has a module including clouds, but we used the clear sky module, to be consistent with the treatment of the other tranmission schemes, while the cloud effect is embedded in $E(0)$.

2.1.3. M02 Scheme

To study the effect of VSR on upper-ocean circulation, Murtugudde et al. (2002) utilized a transmission scheme of VSR based on the bio-optical relationship of Morel (1988). In M02, the penetration of VSR follows an exponential function with depth, with the diffuse attenuation of VSR calculated based on Chl. Specifically, the transmittance of M02 for light in the visible domain is expressed as follows:

$$Tr_{VIS} = e^{-z^*\left(0.027+0.0518Chl^{0.428}\right)} \tag{7}$$

Because the scheme of Murtugudde et al. (2002) calculates only the attenuation of visible light (380–700 nm), the infrared part of M02 used in this study is calculated following the scheme in Lee et al. (2005), and transmission of the two parts is combined as follows:

$$Tr_{M02}(z, Chl) = F_{IR}Tr_{IR} + F_{VIS}Tr_{VIS} \tag{8}$$

where F_{IR} and F_{VIS} are the fractions of solar radiation, with 0.53 for infrared domain (F_{IR}) and 0.47 for visible domain (F_{VIS}) (Frouin et al., 1989).

2.1.4. L05 Scheme

Different from the above *Tr* models using Chl as the input, Lee et al. (2005) developed a transmission scheme (L05) using IOPs. In this IOPs-based scheme, *Tr* is also divided into visible and infrared parts and expressed as follows:

$$Tr_{L05}(z, IOPs, \theta_\alpha) = F_{VIS}e^{-K_{VIS}(IOP,z,\theta_\alpha)z} + F_{IR}e^{-K_{IR}(z,\theta_\alpha)z} \tag{9}$$

where K_{VIS} (m^{-1}) is the attenuation coefficient of VSR (400–700 nm). Note that unlike historical schemes for transmission broadband radiation where K_{VIS} is treated as a constant vertically, K_{VIS} in L05 is modeled as a function of depth (z),

$$K_{VIS}(z, IOP, \theta_a) = K_1(IOP) + \frac{K_2(IOP)}{\sqrt{1+Z}} \tag{10}$$

where K_1 and K_2 are two model parameters, which are described as functions of $a(490)$, $b_b(490)$, and solar zenith angle in the air (θ_α):

$$K_1(IOP, \theta_a) = \left[\chi_0 + \chi_1(a(490))^{0.5} + \chi_2 b_b(490)\right](1 + \alpha_0 sin\theta_\alpha) \tag{11a}$$

$$K_2(IOP, \theta_a) = [\zeta_0 + \zeta_1(a(490)) + \zeta_2 b_b(490)](\alpha_1 + \alpha_2 cos\theta_\alpha) \tag{11b}$$

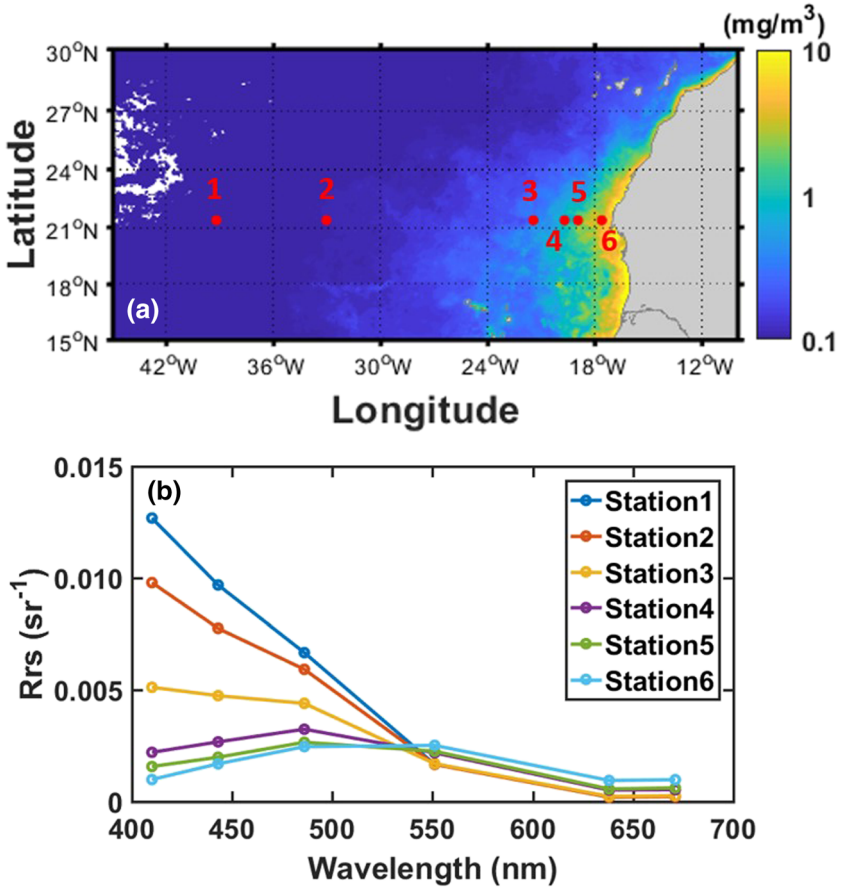

Figure 1. Location of the six stations selected for this study (a) and annual mean Rrs from the visible infrared imaging radiometer suite (VIIRS) (b).

χ_0, χ_1, χ_2, ζ_0, ζ_1, ζ_2, α_0, α_1, and α_2 are model constants tuned by fitting numerical simulations using HydroLight (Mobley, 1995) and can be found in Lee et al. (2005).

The diffuse attenuation coefficient of infrared domain, K_{IR}, is also modeled as a function of depth (z) and sun angle:

$$K_{IR}(z,\theta_a)=\left(0.560+\frac{2.304}{(0.001+z)^{0.65}}\right)(1+0.002\theta_a) \tag{12}$$

Lee et al. (2005) demonstrated that Tr from the L05 scheme matched HydroLight simulations very well for waters with Chl ranging from 0.03 to 30 mg m^{-3} under different sun angles and for depths where VSR is higher than 0.1% of surface VSR.

2.2. 1-D ROMS

We used the ROMS as the physical circulation model to simulate temperature and vertical mixing in the upper water column. The ROMS has been used widely in research on ocean circulation and ecosystem. We used the 1-D version to focus on the effects of different Tr schemes, under the assumption that the influence of mesoscale/submesoscale processes on seasonal upper-ocean heat budget of uniform water mass is not significant. The thickness of the upper layer for the 1-D simulation is set to 200 m, as light contribution at deeper depths is much weaker. This layer is then divided into 100 stretched levels, with

Table 3
Information of the Six Stations and Related Ocean Color Data

Location and water properties	Station					
	1	2	3	4	5	6
Longitude	−36.3125	−26.9375	−21.6875	−19.3958	−18.3125	−17.4792
Latitude	21.4375	21.4375	21.4375	21.4375	21.4375	21.4375
Chl (mg m^{-3})	0.04	0.09	0.29	0.67	1.22	2.04
a(490) (m^{-1})	0.020	0.023	0.044	0.066	0.087	0.13
b_b(490) (m^{-1})	0.0027	0.0027	0.0031	0.0039	0.0045	0.0052
Jerlov water type	IA	IB	II	II	III	III

higher vertical resolution (~0.15 m) close to the surface. Such a setup covers most oceanic waters under a strong impact of solar radiation. Several vertical mixing schemes are incorporated in the ROMS (Robertson & Hartlipp, 2017), and we use the K profile vertical parameterization (Large et al., 1994) in this study.

To evaluate the impact of Tr scheme in different water types, we selected six locations (named Station 1, Station 2, etc.) in the eastern subtropical Atlantic Ocean with significant variations in water color (see Figures 1a and 1b), which suggests a large gradient of Chl to cover different water types (see Figure 1a). Although the six locations span ~1,000 km in distance, they are at the same latitude (21.44 °N); this way, we can use the same solar forcing condition to simply the calculation and discussion. Since our focus is on the impact of Tr scheme with the input derived from ocean color, not on the response of a specific location to broad environmental conditions, we applied the surface forcing (including radiation flux, precipitation, wind, air pressure, and sun angle in a day) of Station 1 (21.44°N, 36.31°W) to all six stations in our model runs. In other words, although the six stations selected in this study are at different locations, they are considered different only in water properties (from clear to turbid), with the estimated Chl changing from ~0.1 to ~2.0 mg m^{-3} from Station 1 to Station 6.

The temperature and salinity data for the initial condition is derived from the Simple Ocean Data Assimilation (SODA) Reanalysis Version 2.0–2.4 (http://iridl.ldeo.colmbia.edu/SOURCES/.CARTONGIESE/SODA/.v2p0p2-4/). The model temperature is not only dependent on solar irradiance, but also influenced by air-sea boundary condition. Daily data for model forcing (including SST, wind, air temperature, and pressure) are from the National Centers for Environmental Prediction (NCEP) reanalysis (https://www.esrl.noaa.gov/psd/data/gridded/data.ncep.reanalysis.surfaceflux.html). The shortwave and longwave radiation fluxes, evaporation, and bottom tracer flux are calculated using analytical formulas in the ROMS.

Using the above mentioned data as initial conditions, we performed 1-D simulations at these six locations using Tr estimated from remote sensing product and the four transmission schemes. We then compared the model results to investigate the impacts of different Tr schemes on temperature and mixing in the upper ocean in different water types.

The required input for these Tr schemes—Chl, a(490) and b_b(490)—were calculated from the same source, namely, the *Visible Infrared Imaging Radiometer Suite* (*VIIRS)* monthly climatology remote sensing reflectance (Rrs; see Figure 1b) (https://oceancolor.gsfc.nasa.gov/l3/). Chl was calculated by using the empirical algorithm in Hu et al. (2012), while a(490) and b_b(490) were calculated by using the quasi-analytical algorithm (QAA) (Lee et al., 2002). As general status indicators of the six stations, the annual mean values of averaged Chl, a(490) and b_b(490) are presented in Table 3. For the PS77 scheme, the water type of every station is determined from the annual mean Chl based on the relationship between Chl and water type proposed by Morel (1988) and fixed for the entire model run as commonly done (Hedström, 2000).

After the model runs were completed, we calculated MLD from the modeled temperature and salinity profiles. Here, we used the density-based definition in Sprintall and Tomczak (1992): the depth where density (σ_t) is equal to the surface σ_t plus the increment in σ_t equivalent to a desired net decrease in temperature (0.5°C).

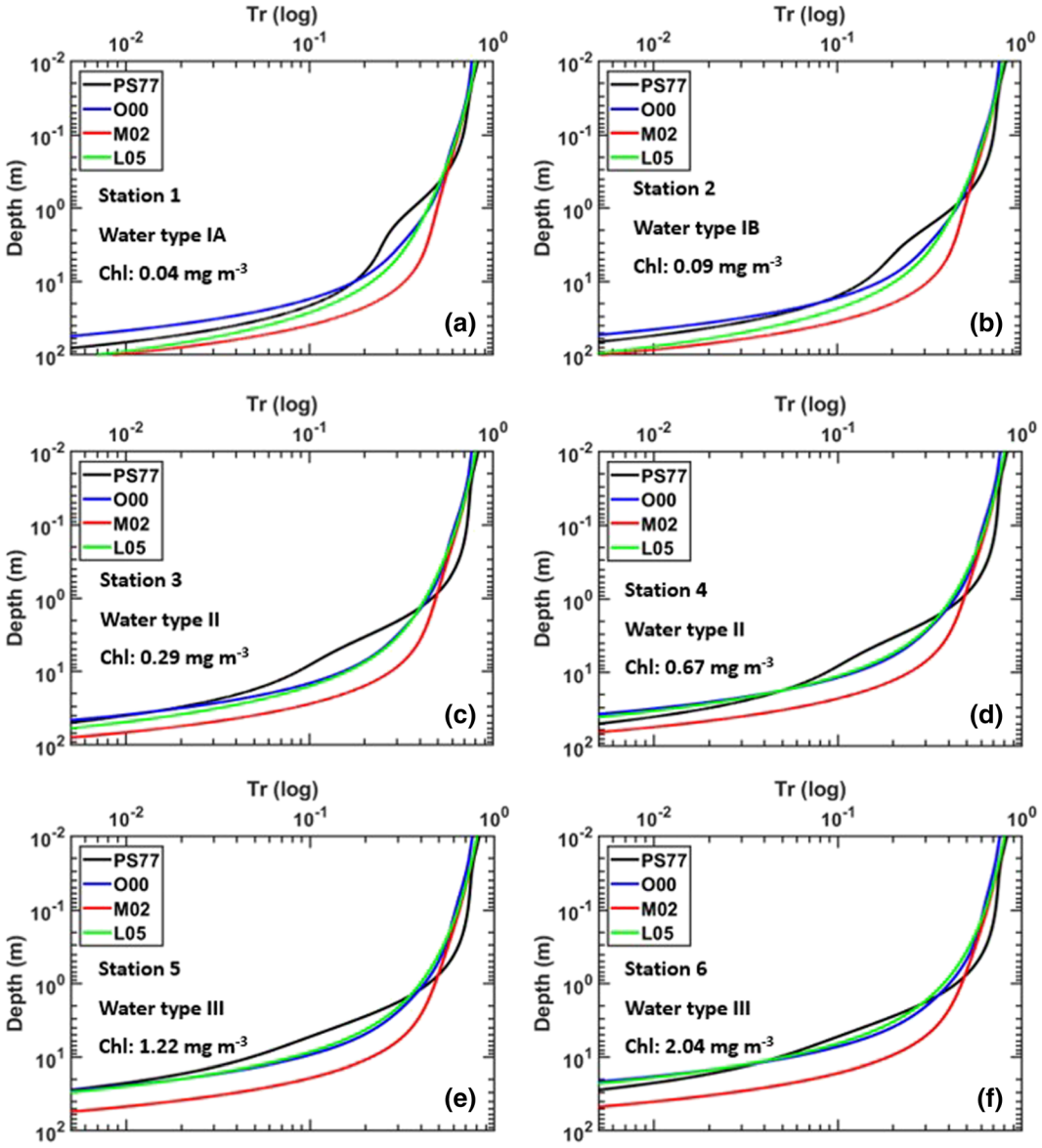

Figure 2. *Tr* of the (a–f) six stations calculated by water type (PS77) and annual mean ocean color data (O00, M02, and L05).

3. Results

3.1. *Tr* Profiles

The *Tr* profiles calculated from ocean color data for the selected sites are presented in Figure 2. Similar to the results shown in Zoffoli et al. (2017), the estimated *Tr* profiles, especially for the depth deeper than ~1 m, are very different from scheme to scheme, although all schemes were based on the same Rrs for each station (see Figure 1b). Generally, *Tr* of PS77 attenuates light more slowly than those of the other three schemes for the first layer (depth < ~1 m) but much faster at deeper depths (> ~2 m) for waters with higher Chl (e.g., water Type III); when the depth gets deeper (depth > 10 m), *Tr* of O00 attenuates faster than those of the other three schemes, and *Tr* of M02 attenuates light generally the slowest. Because K_{VIS} of L05 varies with depth, which effectively accounts for the change of light color with depth and represents better the attenuation nature of broadband solar radiation, *Tr* of L05 attenuates faster in the upper layers and more slowly in the deeper layers compared to *Tr* of PS77 and O00.

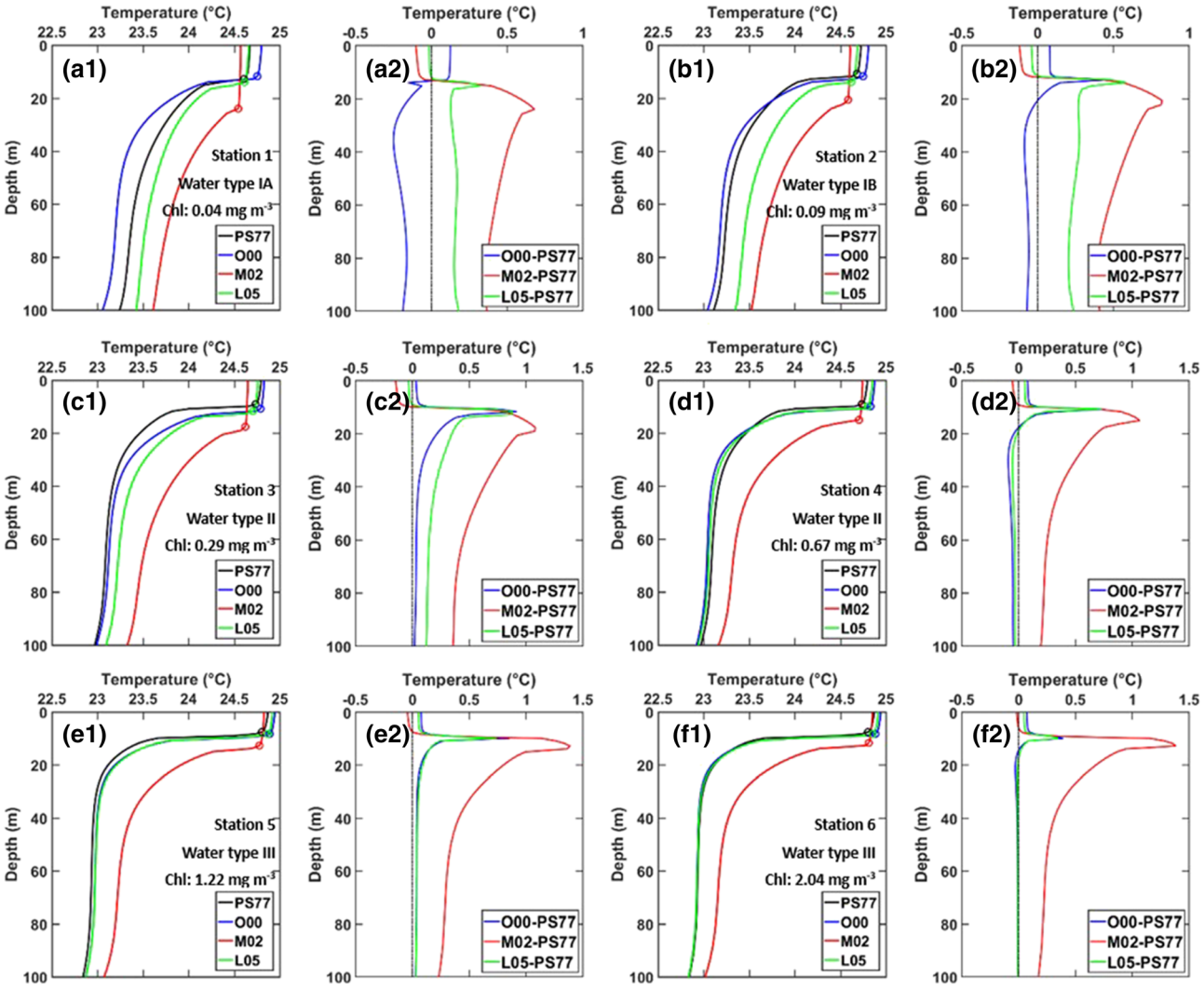

Figure 3. Vertical temperature profiles resulting from the four light transmission models (circles represent the bottom of mixed layer), and the temperature difference between each of the three new models and the default PS77 model, for (a–f) Stations 1–6 in spring (April).

Because a water type covers a range of Chl, the type of water at Station 3 and that at Station 4 are the same (both being Type II), although their Chl and IOPs are quite different (0.29 mg m^{-3} vs. 0.67 mg m^{-3}). This leads to the same *Tr* profiles from PS77 scheme at these two locations but different *Tr* profiles from the other three schemes. The same kind of pattern is observed at Station 5 and Station 6, both being Type III water. Therefore, in the following, besides comparing the impacts of transmission profiles of the four schemes, we also compare the temperature results of Station 3 versus Station 4, and of Station 5 versus Station 6 to highlight the limitations of these schemes based on water types on upper-ocean dynamics.

3.2. Temperature Results

For the four different schemes used to obtain *Tr*, following the convention in ocean circulation simulations (Sweeney et al., 2005; Xiu & Chai, 2014), the models were integrated for 10 years each to obtain stable modeling results for each *Tr* scheme, and we used the results of the tenth year to compare the resulting temperature and MLD. As examples, Figures 3a1, 3b1, 3c1, 3d1, 3e1, and 3f1 show results in spring (April), and Figures 4a1, 4b1, 4c1, 4d1, 4e1, and 4f1 show results in summer (August), along with profiles of temperature difference (Figures 4a2, 4b2, 4c2, 4d2, 4e2, and 4f2) between each of the new *Tr* schemes and the default PS77 *Tr* scheme. As expected, generally there is a mixed layer near the surface where the temperature is

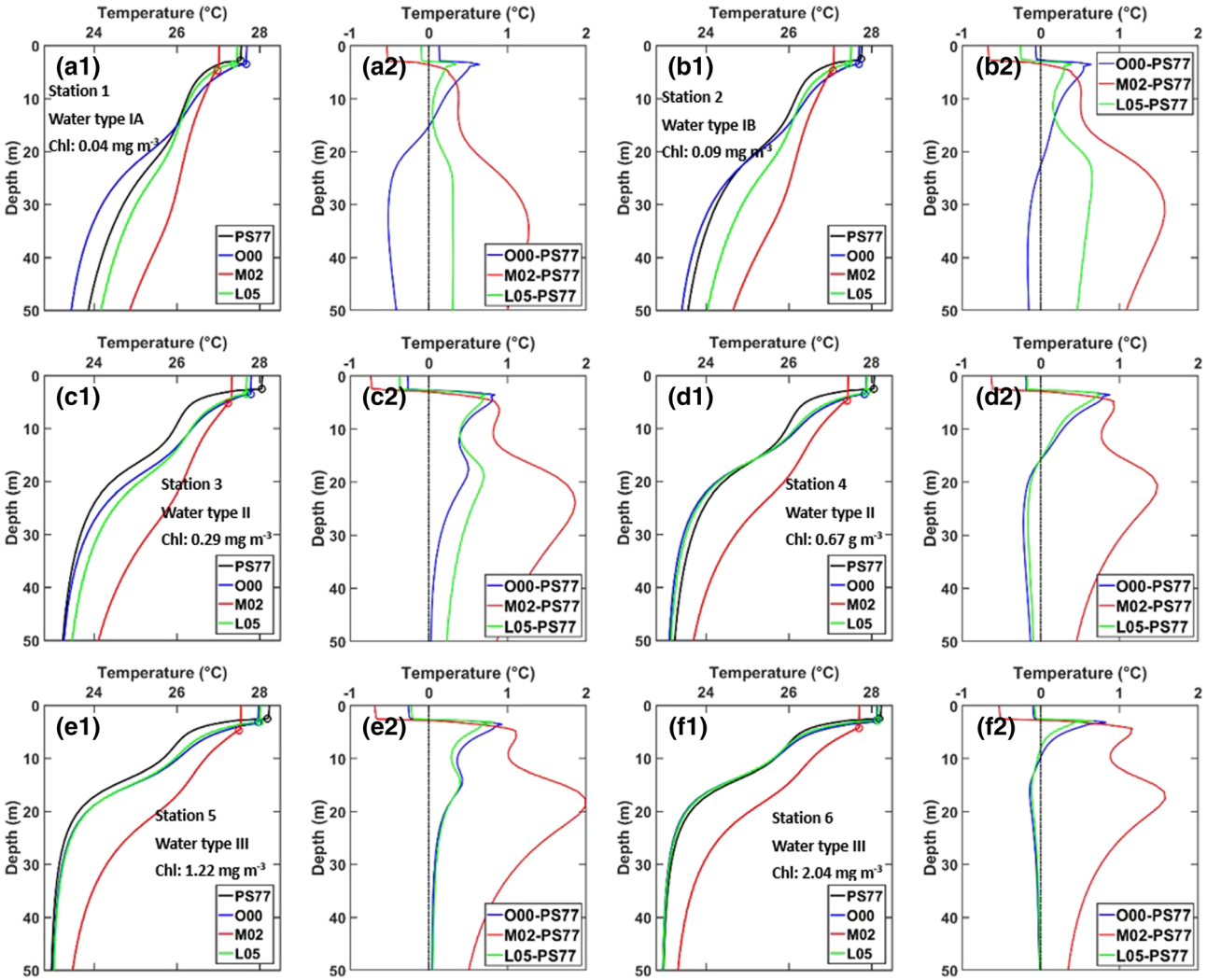

Figure 4. Same as Figure 3, except in summer (August).

nearly uniform; then, temperature decreases rapidly with the increase of depth around the thermocline before becoming stable again.

For the six stations, in general there is a pattern of SST increase (the output temperature at 0-m depth) and MLD decrease when waters change from being clear to being turbid, regardless of the *Tr* scheme used. Using the results from L05 *Tr* as an example, in April SST increases from ~24.6°C to ~24.9°C, while MLD decreases from ~20 to ~17 m for waters changing from clear to turbid. This echoes the finding in the literature (e.g., Jolliff et al., 2012; Nakamoto et al., 2001; Sathyendranath et al., 1991; Shell et al., 2003), that is, more turbid waters trap more solar radiation in the surface layer, subsequently increasing SST and decreasing MLD.

3.2.1. Contrast of Temperature Profiles in Spring

In spring, the upper ocean at our study sites is in the process of being restratified due to increased solar radiation and weaker wind. Compared to winter, mixing becomes weaker and MLD shoals in spring. For all six stations and four *Tr* schemes, the temperatures are around 24.7°C at the surface and around ~23°C at 50 m, but the differences in $T(z)$ profiles among the four *Tr* schemes can be significant (up to ~1.4°C) (see Figure 3), which are significantly larger than the changes of SST (~0.3°C) between clear and turbid waters. Generally, the new *Tr* schemes result in higher $T(z)$ compared to PS77, except for O00 at Station 1 (the clearest water among the six stations). Among them, *Tr* scheme of M02 gives the lowest SST but the deepest MLD, along with the highest $T(z)$ for depths deeper than ~20 m.

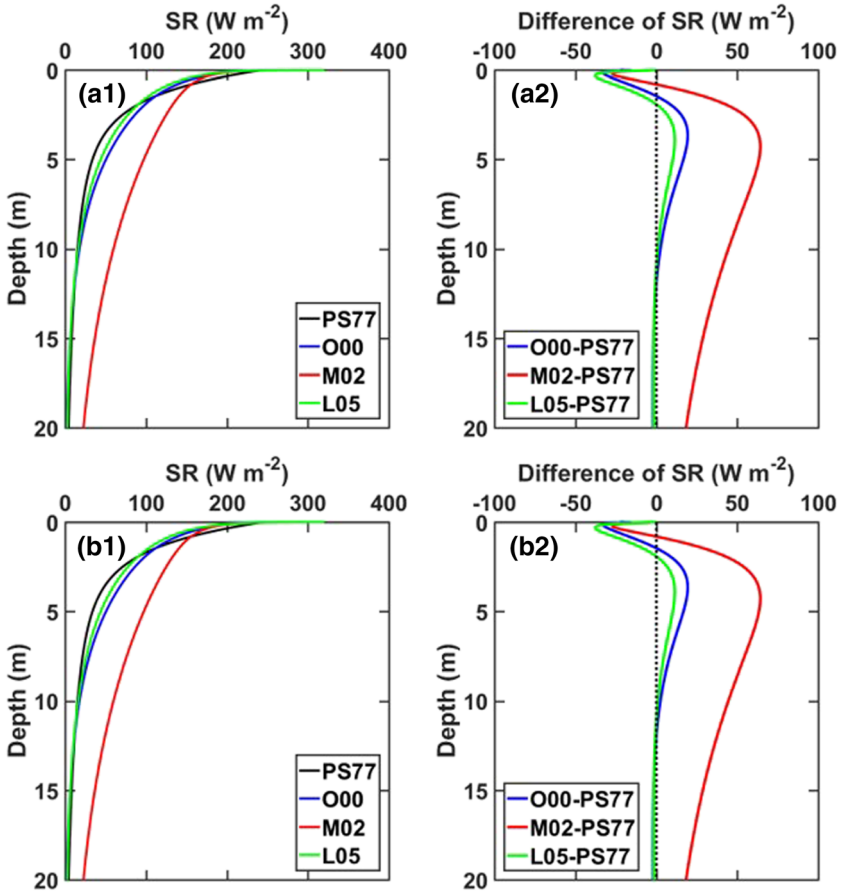

Figure 5. Profiles of daily vertical solar radiation (SR) and the difference of SR between each of the three new schemes and default PS77 at Station 6: (a) spring (1 April), and (b) summer (1 August).

To further assess the impact of *Tr* schemes on upper water column dynamics, we calculated the difference of $T(z)$, using $\Delta T(z) = T(z)^{\text{new scheme}} - T(z)^{\text{PS77}}$, between the results of the new *Tr* schemes and that of the PS77 scheme. The results are included in Figure 3. Generally, $\Delta T(z)$ reaches a maximum near the base of MLD and then decreases with depth as contribution to heating from solar radiation diminishing at deeper depths (e.g., at 300 m). This is likely due to the fact that in the mixed layer, the mixing process redistributes the absorbed energy within this layer, while below the MLD, the transmitted solar radiation at a depth plays a bigger role for temperature at that depth. Also, $\Delta T(0)$ (change of SST) decreases from clear to turbid waters, as photon energy is more concentrated near the surface for more turbid waters, rather spreading out in the upper-ocean water column as it happens for more clear waters.

For Stations 1 to 3 where the remotely estimated Chl is less than ~0.3 mg m^{-3}, $\Delta T(z)$ from the three new *Tr* schemes are found generally in the range of −0.3 to 1.1°C for the upper 100 m. For Stations 4–6, however, $\Delta T(z)$ shows high values (up to 0.8°C) only at depths around the MLD base but decreases sharply below the MLD. This is especially true for Station 6 (Chl ~ 2.0 mg m^{-3}, $a(490)$ ~ 0.13 m^{-1}), a result of the combination of quite similar *Tr* (e.g., between L05 and PS77) and significantly less solar radiation in deeper depths due to strong attenuation in the surface layer.

For all six stations, $\Delta T(z)$ from M02 is the highest (up to 1.4°C) among the three new *Tr* schemes evaluated. This is because of the much slower attenuation of *Tr* of M02 (see Figure 2), especially at depths deeper than ~1 m. This reduced attenuation (which then enhances transmission of solar radiation) results in significantly more energy and consequently higher temperature at deeper depths. As an example, Figure 5a shows the vertical profiles of $E(z)$ and $\Delta E(z)$ (difference of solar radiation between new *Tr* scheme and PS77 *Tr* scheme) at Station 6 on 1 April, where $\Delta E(z)$ is in the range of ~50–70 W m^{-2} for the depth of 2–15 m for the M02

scheme, more than double of those of the O00 and L05 schemes. This significantly enhances the solar radiation at depth from M02, which heats up waters more at deeper depths and hence increases temperature in the deeper layer, further deepening MLD (Figure 4f).

The water type at both Stations 3 and 4 is Type II, but the water properties at the two locations actually differ a lot. For instance, Chl varies from ~0.3 mg m^{-3} at Station 3 to ~0.7 mg m^{-3} at Station 4; that is, Station 4 is more opaque. The *Tr* values of PS77 at these two stations, as they are based on water type, however, are the same. Therefore, the light attenuation in default ROMS simulations will be the same at the two stations, and consequently the impact of solar radiation on the upper-ocean dynamics will not be accurately reflected, at least for one of the stations. The same will be true for Stations 5 and 6, both being Type III but their water properties far from being the same. These results further echo the necessity and importance of incorporating satellite ocean color product to improve ocean circulation modeling (Nakamoto et al., 2001; Shell et al., 2003).

3.2.2. Contrast of Temperature Profiles in Summer

In summer, mixing in the upper layer is the weakest and stratification is the strongest due to strong solar radiation and weak wind. Therefore, the effect of *Tr* on upper-ocean temperature is most significant. As shown in Figure 4, all six stations show SST of ~27–28°C in summer for the *Tr* schemes used, while it may be higher (by ~0.2°C, Station 1 with O00 only) or lower (~up to −0.7°C), depending on the *Tr* scheme used. Also, due to stratification, much shallower MLD values (by ~2–5 m, shallower for more turbid waters) are observed in these waters. Further, $T(z)$ varies significantly from clear to turbid waters because of different solar heating at deeper depths. For example, $T(30)$ is ~24–25°C at Station 1 (except for the result of M02), but only ~23°C at Station 6 (except for the result of M02).

Again, $\Delta T(z)$ was calculated for each *Tr* scheme, and the results are included in Figure 4. Similar to the results in spring, except for M02, the highest $\Delta T(z)$ is found around the MLD base, and $\Delta T(z)$ decreases sharply for depths below the MLD. The differences generally decrease when waters change from clear to turbid (except for the result of M02), a result of less photon energy reaching deeper depths to heat up water.

The *Tr* scheme of M02 results in the largest impact on the $T(z)$ profile, with lower $T(z)$ for depths above the MLD ($\Delta T(0) \sim -0.5$°C for the six stations), while significantly higher $T(z)$ is seen for depths below the MLD ($\Delta T(20)$ up to ~2.0°C at the six stations). As observed in spring, this is the result of the significantly enhanced solar radiation at depths from the M02 scheme. For example, $E(20)$ can be ~30 W m^{-2} at Station 6 from the M02 scheme on 1 August, but it is <5 W m^{-2} for the other three *Tr* schemes (see Figure 5b). For those clearer waters (Stations 1–3, Chl < ~0.3 mg m^{-3}), the $\Delta T(z)$ values of O00 and L05 are not as high as that of M02, but still in the range of ~ − 0.5–1.0°C, sufficient to change the mixing of water parcels in the upper water column. Although all *Tr* values were computed from the same Rrs spectrum at each station, their different impacts on temperature and MLD further emphasize the importance of *Tr* scheme on ocean circulation modeling and understanding of upper-ocean dynamics.

3.2.3. Monthly SST

The monthly averaged SST from the four *Tr* schemes and their differences are shown in Figure 6. Because the forcing conditions at each station may not exactly represent the true conditions at the location selected in this study, the temporal variations of the resulting SST of these six stations do not necessarily match those observed. Nevertheless, for waters changing from clear to turbid, SST (from all four *Tr* schemes) in summer is found increased (by ~0.85°C at all locations), matching the expectation that more photons are absorbed in the surface layer by turbid waters. There is a larger difference in $\Delta T(0)$ (SST) for clearer waters, while this difference is significantly smaller (except for M02) for more turbid waters (e.g., Station 6). Further, although all four schemes show increases of SST from winter to summer, the temporal changes in SST are not uniform among the *Tr* schemes used. For instance, SST at Station 1 increases by ~4.2°C with the O00 scheme, but by ~3.0°C with the M02 scheme. These results clearly indicate a strong dependence of surface properties on the *Tr* scheme used.

3.3. MLD

MLD is one of the most important variables to describe the upper-ocean state. This depth is directly related to SST and nutrient utilization and consequently affects phytoplankton dynamics and biological productivity in the ocean (Sverdrup, 1953). Solar radiation can significantly affect MLD (Gnanadesikan & Anderson, 2009; Liang & Wu, 2013; Nakamoto et al., 2001); therefore, we compare MLD sensitivity to *Tr* scheme here.

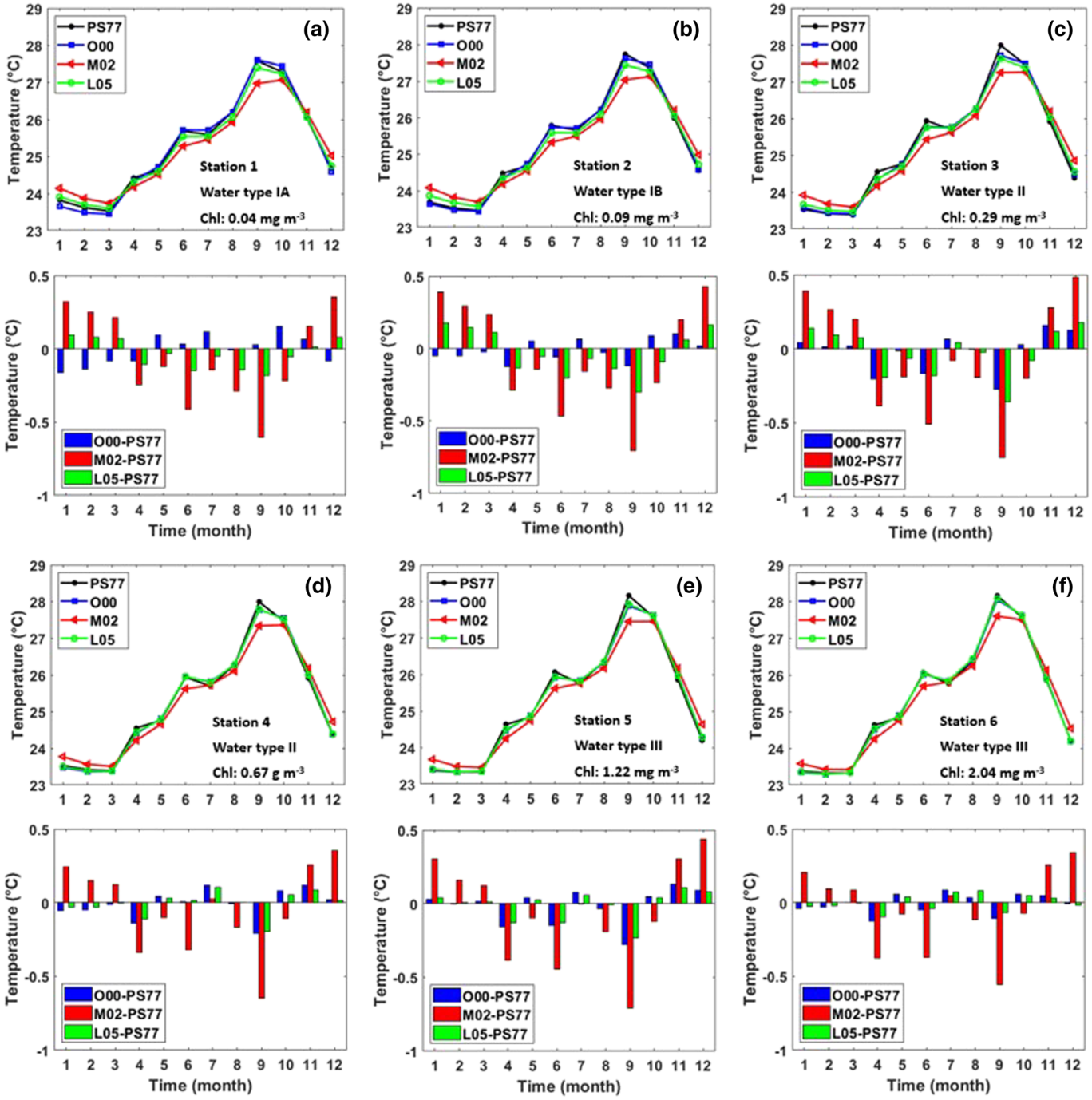

Figure 6. Monthly SSTs from the four light transmission schemes at (a–f) Stations 1–6, and the differences of SST between each new scheme and PS77.

Figure 7 shows the MLD results from the four *Tr* schemes and the differences of MLD between each of the new *Tr* schemes and PS77 ($\Delta MLD = MLD^{new\ scheme} - MLD^{PS77}$). Again, because the forcing may not be realistic at all six locations, the temporal variation of the resulting MLD at each station may not be necessarily matching that observed for the locations selected. However, the general pattern of deeper MLD in winter and shallower MLD in summer is consistent with our knowledge of upper-ocean dynamics. Note that the results do show significant impact of *Tr* schemes on MLD. For instance, modeled MLD shows a difference of ~10–20 m in January, and up to ~30 m in May, between the new *Tr* schemes and PS77 at the six locations. Also, as observed for SST, the seasonal patterns of ΔMLD between the three new *Tr* schemes and PS77 are

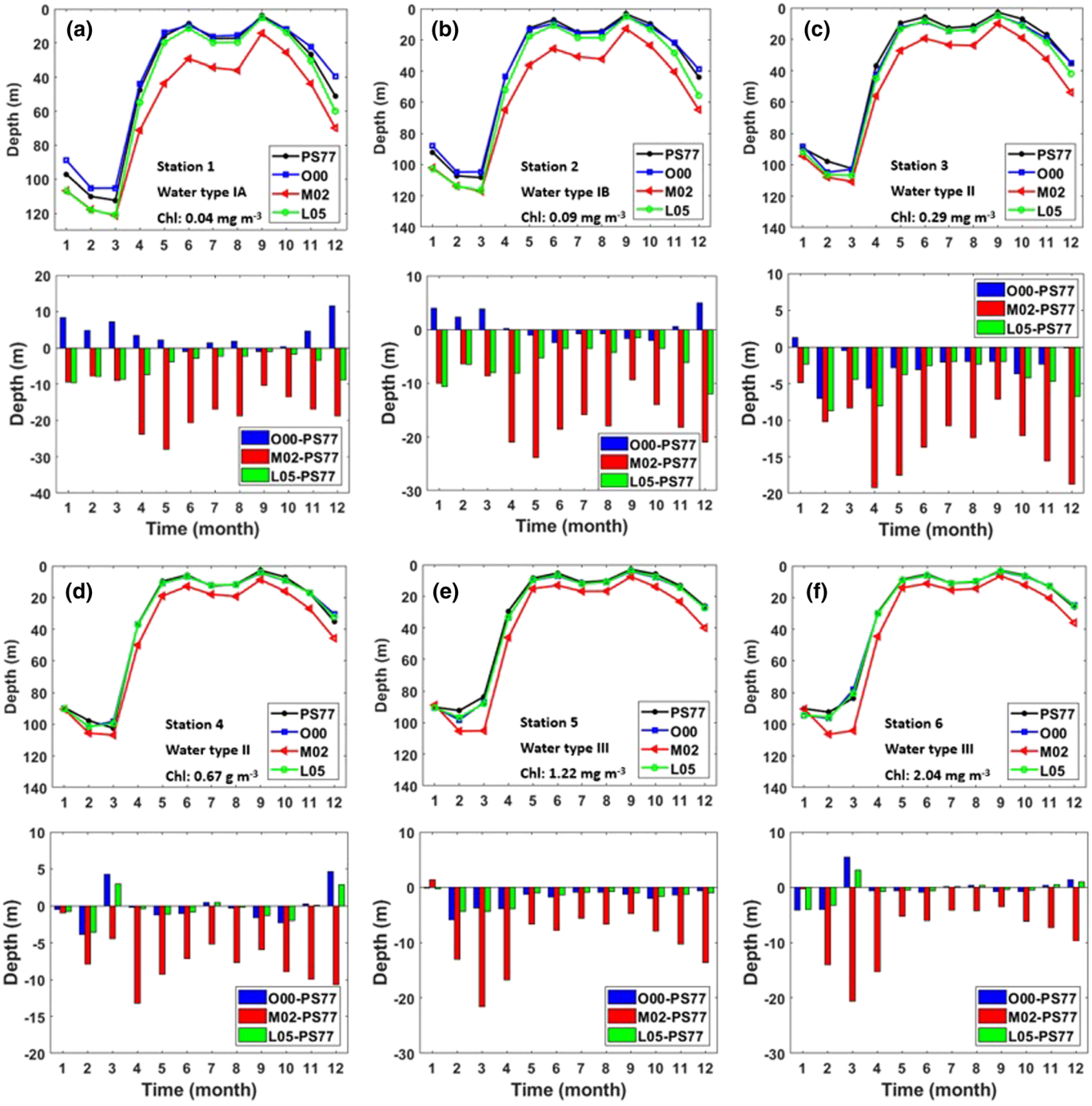

Figure 7. Same as Figure 6, except for MLD.

very different. For instance, for Station 4 (see Figure 7d), using the results of PS77 as a reference, the MLD values from the new *Tr* schemes are deeper by ~4–8 m in February, but the MLD values from O00 and L05 are shallower by ~3–5 m in March, while the MLD from M02 is deeper by ~5 m.

Again, for all the locations and all months (except at Station 5 in January), the results of M02 show the deepest MLD among the four *Tr* schemes tested. As discussed regarding $\Delta T(z)$ and SST, this is the result of significantly weaker attenuation by the M02 scheme, which results in more photon energy and higher $T(z)$ in deeper depths (see Figure 5). This will normally lead to deeper MLD, as MLD is determined mainly by the $T(z)$ profile (see section 2.2).

Further, between the MLD results of Stations 3 and 4 (Figures 7c and 7d), because the water at Station 4 is more turbid, its MLD values from the new *Tr* schemes are shallower than those of Station 3 by 5–10 m, while the MLD values from PS77 are the same at these two locations. Similar results are found at Stations 5 and 6, which further indicates the limitation and significant impact of water-type-based *Tr* scheme on ocean circulation modeling.

4. Discussion

4.1. Essential Difference Between Chl-Based and IOPs-Based Schemes for *Tr* Estimated From Rrs

It has long been recognized that since visible light can penetrate deep into the upper ocean to heat up water in this layer, it is important to consider this portion of the solar radiation differently from the entire visible-shortwave solar energy in dynamic ocean models. Subsequently, schemes have been developed to propagate VSR from surface to deeper depths. Most ROMS simulations adopted the Paulson and Simpson (1977) scheme from the 1980s and onward. The default *Tr* scheme in ROMS sometimes even simply applies one water type at all grids from open ocean to nearshore waters, which is certainly far from reality. With the availability of satellite ocean color remote sensing, it is essential to incorporate these large-scale observations into ocean circulation modeling. However, there is no direct, one-step conversion between observed ocean color (Rrs) and $Tr(z)$; rather this application of ocean color measurement is through a "middle man," conventionally via Chl.

A scheme based on Chl to map Jerlov water type was developed decades ago (Morel, 1988), which allows different pixels to have different water types. The scheme can be incorporated into the ROMS. Further, various schemes (Morel, 1988; Morel & Antoine, 1994; Ohlmann & Siegel, 2000) were developed, which directly use Chl as the input to model the penetration of the visible light or the entire visible-shortwave radiation. When these schemes are incorporated into regional or global circulation models (Jolliff et al., 2012; Lin et al., 2007; Shell et al., 2003; Zhang et al., 2011), because the only available and measured information for estimating $Tr(z)$ is Rrs spectrum, the accuracy of the estimated *Tr* depends on two independent components or modules: Chl from Rrs, and *Tr* based on Chl. Because Rrs and *Tr* are optical properties and Chl is a biological property, the process from Rrs to *Tr* (Chl, z) includes two bio-optical conversions, along with several independent parameters involved in the conversions. As detailed in Appendix A, these parameters are not constant; thus, they will bring in various uncertainties in the estimated *Tr* from Rrs spectrum. However, because both Rrs and IOPs are optical properties, deriving *Tr* (IOPs, z) from Rrs is more direct, and there is no involvement of bio-optical conversions (see Appendix A for more detailed discussion). Therefore, there are significant differences between Chl-based and IOPs-based schemes for *Tr* from Rrs, and IOPs-based schemes have advantages.

4.2. Implications for Basin-Scale Circulation Modeling

It has been demonstrated long ago (Sathyendranath et al., 1991) and echoed by several studies (Liang & Wu, 2013; Mobley et al., 2015; Morel & Antoine, 1994; Nakamoto et al., 2001; Shell et al., 2003) that it is important to take into account the effect of VSR in circulation models. For basin-scale studies, however, the available measurement is ocean color (represented by an Rrs spectrum, see Figure 1b), while Chl or IOPs are derived (or estimated) from such a spectrum. Thus, effectively and accurately using Rrs information in basin-scale circulation models is the key. Here, although we only evaluated six stations with different Rrs spectrum (indicating different water properties), our results do indicate significant impact on upper-ocean dynamics from different *Tr* schemes. This is especially true for clearer waters (Chl < ~0.3 mg m^{-3}), where a change in *Tr* will result in significantly different photon energy at deeper depths. When this change in solar radiation is greater than the energy exchange from ocean mixing, it will then have a big impact on $T(z)$ and MLD. For more turbid waters, because of reduced contribution of solar radiation at deeper depths, the impact of *Tr* scheme is less significant at deeper depths. However, based on satellite ocean color remote sensing, more than ~75% of the global ocean has Chl < 0.3 mg m^{-3} (see Figure 8). This suggests that a proper *Tr* scheme is critical for basin-scale circulation modeling, where the only available measurement from ocean color satellite is the Rrs spectrum.

Furthermore, in this study the influence of different *Tr* schemes is only investigated using a 1-D model for 10-year integration. When the scheme is applied to long-term basin-scale circulation models, wrong choice of *Tr* scheme could result in bigger errors of subsurface heat content calculation.

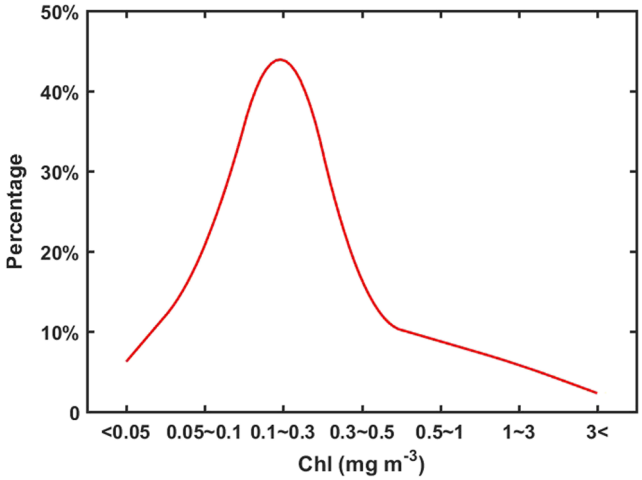

Figure 8. Histogram of global Chl concentration (calculated from MODIS annual Chl product of 2018).

5. Summary

In this work, the influence of VSR transmission scheme on temperature and mixing in the upper ocean is investigated using the well-known 1-D ROMS. We chose six stations representing different water properties (i.e., light absorption capacity) and applied the same initial parameters and forcing conditions but different *Tr* schemes. These *Tr* schemes use Chl or IOPs as input, with the input derived from the same measured Rrs. Thus, any resulting differences in temperature and mixing are solely from the scheme used in modeling *Tr*.

It is found that although all *Tr* estimates are from the same satellite Rrs, different VSR transmission schemes can lead to significant differences in vertical temperature profile and MLD, with maximum differences in temperature up to 2°C and maximum differences in MLD up to ~30 m. These changes are equivalent or higher than the contribution of taking into account solar radiation. Such finding emphasizes the importance to accurately describe VSR transmission as it can significantly impact upper-ocean dynamics, especially for clear waters where there could still have a large amount of VSR at hundreds of meters below the surface.

Further, because ocean color remote sensing measures water's optical properties and light attenuation is governed also by optical properties (absorption and scattering coefficients) of the bulk water, these results further highlight the broad applicability of transmission scheme centered on IOPs, where the uncertainties associated with bio-optical conversions are avoided. Although the results here were drawn from 1-D modeling, we envision that significantly improved results in upper-ocean dynamics would emerge when IOPs-based transmission schemes are applied to 3-D global ocean circulation models.

Data Availability Statement

The data are available online (at https://oceancolor.gsfc.nasa.gov/l3/). The SODA ocean temperature data and the NCEP daily forcing data used in this study are obtained from http://iridl.ldeo.columbia.edu/SOURCES/.CARTON-GIESE/SODA/.v2p0p2-4/ and https://www.esrl.noaa.gov/psd/data/gridded/data.ncep.reanalysis.surfaceflux.html, respectively.

Appendix A: Fundamental Differences Between *Tr* (Chl) and *Tr* (IOPs)

Although the "middle man" between observed Rrs and $Tr(z)$ is conventionally Chl in the past decades of research, Rrs never directly provides a measure of Chl. It has been shown that Rrs is fundamentally a function of the total absorption (a) and backscattering (b_b) coefficients, which can generally be expressed as follows:

$$\mathrm{Rrs} = G\frac{b_b}{a} \tag{A1}$$

where G is a model parameter for Rrs, which can generally be approximated as a constant (Gordon et al., 1988; Morel & Gentili, 1991). Thus, the first-order inversion from an Rrs spectrum are a and b_b (IOCCG, 2005; Lee et al., 2002). To estimate Chl from Rrs, both a and b_b must be modeled explicitly (semi-analytical algorithms) or implicitly (empirical algorithms) as a function of Chl, and Equation A1 become,

$$\mathrm{Rrs} = G\frac{f_1(\beta^*, \mathrm{Chl})}{f_2(\alpha^*, \mathrm{Chl})} \tag{A2}$$

with α^* and β^* being the model coefficients to convert Chl to a and b_b, respectively. In other words, when Chl is estimated from Rrs, it is in general a function as follows:

$$\mathrm{Chl} = f_3(\alpha^*, \beta^*, \mathrm{Rrs}) \tag{A3}$$

In this dependence, values of α^* and β^* are far from constant (Bricaud et al., 1995; Loisel et al., 2010).

Further, when the attenuation coefficient of solar radiation (K_{SR}) is modeled as a function of Chl, a process that is independent of the development of the Chl inversion algorithm from Rrs, there is

$$K_{SR}(\mathrm{Chl}) = f_4(\mathrm{Chl}) \tag{A4a}$$

Because K_{SR} is an optical property, while Chl is a biological property, the conversion of Chl to K_{SR}, explicitly or implicitly, also requires conversions from a biological property to optical properties, normally termed as Chl-specific absorption coefficient (a^*_{Chl}) and Chl-specific backscattering coefficient (b^*_b). So, Equation A4a actually is

$$K_{SR}(\mathrm{Chl}) = f_4\left(a^*_{Chl}, b^*_b, \mathrm{Chl}\right) \tag{A4b}$$

Again, the values of a^*_{Chl} and b^*_b are not constant; rather, they vary significantly from waters to waters (Bricaud et al., 1995; Morel & Antoine, 1994).

When Chl of Equation A3 is applied to a Chl-based scheme (Equation A4b) for K_{SR}, a step required to apply satellite measurements for modeling basin-scale dynamics, it becomes

$$K_{SR}(\mathrm{Chl}) = f_4\left(a^*_{Chl}, b^*_b, \alpha^*, \beta^*, \mathrm{Rrs}\right). \tag{A5}$$

Thus, we see at least four modeling parameters (a^*_{Chl}, b^*_b, α^*, β^*) associated with the two independent steps when Rrs is the sole source for estimating K_{SR}, where there is never a guarantee that the variations of the four parameters will cancel out. The variation and mismatch of these modeling parameters in part explain the different results among the three *Tr* schemes based on Chl.

When K_{SR} is modeled as a function of water's IOPs (in particular the total absorption and backscattering coefficients) (Gordon, 1989; Lee et al., 2005; Sathyendranath & Platt, 1989), from the radiative transfer in general, there is

$$K_{SR}(\mathrm{IOPs}) = h_1(a, b_b) \tag{A6}$$

In this relationship, K_{SR} as well as a and b_b are optical properties, where there is no involvement of bio-optical conversions. Further, a and b_b can be inverted from an Rrs spectrum (Lee et al., 2002; Loisel & Stramski, 2000), which generally can be expressed as

$$a = h_2(\mathrm{Rrs}) \tag{A7a}$$

$$b_b = h_3(\mathrm{Rrs}) \tag{A7b}$$

So, Equation A6 in essence is

$$K_{SR}(\mathrm{IOPs}) = h_4(\mathrm{Rrs}) \tag{A8}$$

Comparing Equation A8 with Equation A5, because a^*_{Chl} will not necessarily be canceled out by α^*, and b^*_b not necessarily be canceled out by β^*, regardless of the accuracy of IOPs or Chl estimated from an Rrs spectrum, compared to the K_{SR}(Chl) model, K_{SR}(IOPs) models will at least avoid the four bio-optical variables (a^*_{Chl}, b^*_b, α^*, β^*) when Rrs is the sole input for the calculation of K_{SR}. The above mentioned fundamental differences between *Tr* (Chl) and *Tr* (IOPs) provide a solid base for understanding the significant differences between different schemes regarding *Tr* estimate, and the advantages of *Tr* (IOPs) (Zoffoli et al., 2017), although all are calculated from the same Rrs spectrum.

Acknowledgments

Financial support from the Chinese Ministry of Science and Technology (2016YFC1400905, 2016YFA0601201, and 2016YFC1401601), the National Natural Science Foundation of China (41830102, 41890803, 41730536, and 41890805), the Joint Polar Satellite System (JPSS) funding for the NOAA ocean color calibration and validation (Cal/Val) project, and the University of Massachusetts Boston is greatly appreciated. The authors wish to thank the NOAA/STAR for providing the VIIRS data.

References

Bricaud, A., Babin, M., Morel, A., & Claustre, H. (1995). Variability in the chlorophyll-specific absorption coefficients of natural phytoplankton: Analysis and parameterization. *Journal of Geophysical Research*, *100*(C7), 13,321–13,332. https://doi.org/10.1029/95JC00463

Frouin, R., Lingner, D. W., Gautier, C., Baker, K. S., & Smith, R. C. (1989). A simple analytical formula to compute clear sky total and photosynthetically available solar irradiance at the ocean surface. *Journal of Geophysical Research*, *94*(C7), 9731–9742. https://doi.org/10.1029/JC094iC07p09731

Fujii, M., Boss, E., & Chai, F. (2007). The value of adding optics to ecosystem models: A case study. *Biogeosciences Discussions*, *4*(3), 1585–1631. https://doi.org/10.5194/bgd-4-1585-2007

Gnanadesikan, A., & Anderson, W. G. (2009). Ocean water clarity and the ocean general circulation in a coupled climate model. *Journal of Physical Oceanography*, *39*(2), 314–332. https://doi.org/10.1175/2008JPO3935.1

Gordon, H. R. (1989). Dependence of the diffuse reflectance of natural waters on the sun angle. *Limnology and Oceanography*, *34*(8), 1484–1489. https://doi.org/10.4319/lo.1989.34.8.1484

Gordon, H. R., Brown, O. B., Evans, R. H., Brown, J. W., Smith, R. C., Baker, K. S., & Clark, D. K. (1988). A semianalytic radiance model of ocean color. *Journal of Geophysical Research*, *93*(D9), 10,909–10,924. https://doi.org/10.1029/JD093iD09p10909

Hedström, K. (2000). *Technical manual for a coupled sea-ice/ocean circulation model*. Anchorage, Alaska: MMS.

Hu, C., Lee, Z., & Franz, B. (2012). Chlorophyll a algorithms for oligotrophic oceans: A novel approach based on three-band reflectance difference. *Journal of Geophysical Research*, *117*, C01011. https://doi.org/10.1029/2011jc007395

IOCCG (2005). Ocean-colour bio-optical algorithms. In Z. P. Lee (Ed.), *IOCCG Report Series, no. 5* (pp. 1–122). Dartmouth, Canada: International Ocean Colour Coordinating Group.

IOCCG (2020). Synergy between ocean colour and biogeochemical/ecosystem models. In S. Dutkiewicz (Ed.), *IOCCG Report Series, no. 19* (pp. 1–194). Dartmouth, Canada: International Ocean Colour Coordinating Group.

Jerlov, N. G. (1968). *Optical oceanography* (p. 194). Amsterdam, The Netherlands: Elsevier.

Jolliff, J. K., Smith, T. A., Barron, C. N., deRada, S., Anderson, S. C., Gould, R. W., & Arnone, R. A. (2012). The impact of coastal phytoplankton blooms on ocean-atmosphere thermal energy exchange: Evidence from a two-way coupled numerical modeling system. *Geophysical Research Letters*, *39*, L24607. https://doi.org/10.1029/2012GL053634

Kou, L., Labrie, D., & Chylek, P. (1993). Refractive indices of water and ice in the 0.65- to 2.5-μm spectral range. *Applied Optics*, *32*(19), 3531–3540. https://doi.org/10.1364/AO.32.003531

Large, W. G., McWilliams, J. C., & Doney, S. C. (1994). Oceanic vertical mixing: A review and a model with a nonlocal boundary layer parameterization. *Reviews of Geophysics*, *32*(4), 363–403. https://doi.org/10.1029/94RG01872

Lee, Z., Arnone, R., Hu, C., Werdell, P. J., & Lubac, B. (2010). Uncertainties of optical parameters and their propagations in an analytical ocean color inversion algorithm. *Applied Optics*, *49*(3), 369–381. https://doi.org/10.1364/AO.49.000369

Lee, Z., Carder, K. L., & Arnone, R. A. (2002). Deriving inherent optical properties from water color: A multiband quasi-analytical algorithm for optically deep waters. *Applied Optics*, *41*(27), 5755–5772. https://doi.org/10.1364/AO.41.005755

Lee, Z., Du, K., Arnone, R., Liew, S., & Penta, B. (2005). Penetration of solar radiation in the upper ocean: A numerical model for oceanic and coastal waters. *Journal of Geophysical Research*, *110*, C09019. https://doi.org/10.1029/2004JC002780

Lewis, M. R., Carr, M. E. G., Feldman, C., Esaias, W., & McClain, C. (1990). Influence of penetrating solar radiation on the heat budget of the equatorial Pacific Ocean. *Nature*, *347*(6293), 543–545. https://doi.org/10.1038/347543a0

Liang, X., & Wu, L. (2013). Effects of solar penetration on the annual cycle of sea surface temperature in the North Pacific. *Journal of Geophysical Research: Oceans*, *118*, 2793–2801. https://doi.org/10.1002/jgrc.20208

Lin, P., Liu, H., & Zhang, X. (2007). Sensitivity of the upper ocean temperature and circulation in the equatorial Pacific to solar radiation penetration due to phytoplankton. *Advances in Atmospheric Sciences*, *24*(5), 765–780. https://doi.org/10.1007/s00376-007-0765-7

Loisel, H., Lubac, B., Dessailly, D., Duforet-Gaurier, L., & Vantrepotte, V. (2010). Effect of inherent optical properties variability on the chlorophyll retrieval from ocean color remote sensing: An in situ approach. *Optics Express*, *18*(20), 20,949–20,959. https://doi.org/10.1364/OE.18.020949

Loisel, H., & Stramski, D. (2000). Estimation of the inherent optical properties of natural waters from the irradiance attenuation coefficient and reflectance in the presence of Raman scattering. *Applied Optics*, *39*(18), 3001–3011. https://doi.org/10.1364/AO.39.003001

Mecherikunnel, A. T., & Richmond, J. (1980). *Spectral distribution of solar radiation* (pp. 1–93). Greenbelt, MD: NASA.

Mobley, C. D. (1994). *Light and water: Radiative transfer in natural waters*. Cambridge, MA: Academic Press.

Mobley, C. D. (1995). *Hydrolight 3.0 users guide*. Menlo Park, CA: SRI International.

Mobley, C. D., Chai, F., Xiu, P., & Sundman, L. K. (2015). Impact of improved light calculations on predicted phytoplankton growth and heating in an idealized upwelling-downwelling channel geometry. *Journal of Geophysical Research: Oceans*, *120*, 875–892. https://doi.org/10.1002/2014JC010588

Morel, A. (1988). Optical modeling of the upper ocean in relation to its biogenous matter content (case I waters). *Journal of Geophysical Research*, *93*(C9), 10,749–10,768. https://doi.org/10.1029/JC093iC09p10749

Morel, A., & Antoine, D. (1994). Heating rate within the upper ocean in relation to its bio-optical state. *Journal of Physical Oceanography*, *24*(7), 1652–1665. https://doi.org/10.1175/1520-0485(1994)024<1652:HRWTUO>2.0.CO;2

Morel, A., & Gentili, B. (1991). Diffuse reflectance of oceanic waters: Its dependence on sun angle as influenced by the molecular scattering contribution. *Applied Optics*, *30*(30), 4427–4438. https://doi.org/10.1364/AO.30.004427

Murtugudde, R., Beauchamp, J., McClain, C. R., Lewis, M., & Busalacchi, A. J. (2002). Effects of penetrative radiation on the upper tropical ocean circulation. *Journal of Climate*, *15*(5), 470–486. https://doi.org/10.1175/1520-0442(2002)015<0470:EOPROT>2.0.CO;2

Nakamoto, S., Kumar, S. P., Oberhuber, J. M., Ishizaka, J., Muneyama, K., & Frouin, R. (2001). Response of the equatorial Pacific to chlorophyll pigment in a mixed layer isopycnal ocean general circulation model. *Geophysical Research Letters*, *28*(10), 2021–2024. https://doi.org/10.1029/2000GL012494

Ohlmann, J. C., & Siegel, D. A. (2000). Ocean radiant heating. Part II: Parameterizing solar radiation transmission through the upper ocean. *Journal of Physical Oceanography*, *30*(8), 1849–1865. https://doi.org/10.1175/1520-0485(2000)030<1849:ORHPIP>2.0.CO;2

Paulson, C. A., & Simpson, J. J. (1977). Irradiance measurements in the upper ocean. *Journal of Physical Oceanography*, *7*(6), 952–956. https://doi.org/10.1175/1520-0485(1977)007<0952:IMITUO>2.0.CO;2

Ricchiazzi, P., Yang, S., Gautier, C., & Sowle, D. (1998). SBDART: A research and teaching software tool for plane-parallel radiative transfer in the Earth's atmosphere. *Bulletin of the American Meteorological Society*, *79*(10), 2101–2114. https://doi.org/10.1175/1520-0477(1998)079<2101:SARATS>2.0.CO;2

Robertson, R., & Hartlipp, P. (2017). Surface wind mixing in the regional ocean modeling system (ROMS). *Geoscience Letters*, *4*(1), 24. https://doi.org/10.1186/s40562-017-0090-7

Sathyendranath, S., Gouveia, A. D., Shetye, S. R., Ravindran, P., & Platt, T. (1991). Biological control of surface temperature in the Arabian Sea. *Nature*, *349*(6304), 54–56. https://doi.org/10.1038/349054a0

Sathyendranath, S., & Platt, T. (1989). Computation of aquatic primary production: Extended formalism to include effect of angular and spectral distribution of light. *Limnology and Oceanography*, *34*(1), 188–198. https://doi.org/10.4319/lo.1989.34.1.0188

Sathyendranath, S., Prieur, L., & Morel, A. (1989). A three-component model of ocean colour and its application to remote sensing of phytoplankton pigments in coastal waters. *International Journal of Remote Sensing*, *10*(8), 1373–1394. https://doi.org/10.1080/01431168908903974

Shell, K. M., Frouin, R., Nakamoto, S., & Somerville, R. C. J. (2003). Atmospheric response to solar radiation absorbed by phytoplankton. *Journal of Geophysical Research*, *108*(D15), 4445. https://doi.org/10.1029/2003JD003440

Shulman, I., Gould, R. W., Anderson, S., & Sakalaukus, P. (2017). Impact of errors in short wave radiation and its attenuation on modeled upper ocean heat content. *Journal of Applied Remote Sensing*, *11*(3), 032402. https://doi.org/10.1117/1.JRS.11.032402

Sprintall, J., & Tomczak, M. (1992). Evidence of the barrier layer in the surface layer of the tropics. *Journal of Geophysical Research*, *97*(C5), 7305–7316. https://doi.org/10.1029/92JC00407

Sverdrup, H. U. (1953). On conditions for the vernal blooming of phytoplankton. *Journal du Conseil Permanent International pour l'Exploration de la Mer*, *18*(3), 287–295. https://doi.org/10.1093/icesjms/18.3.287

Sweeney, C., Gnanadesikan, A., Griffies, S. M., Harrison, M. J., Rosati, A. J., & Samuels, B. L. (2005). Impacts of shortwave penetration depth on large-scale ocean circulation and heat transport. *Journal of Physical Oceanography*, *35*, 1103–1106, 1119. https://doi.org/10.1175/jpo2740.1

Xiu, P., & Chai, F. (2014). Connections between physical, optical and biogeochemical processes in the Pacific Ocean. *Progress in Oceanography*, *122*, 30–53. https://doi.org/10.1016/j.pocean.2013.11.008

Zaneveld, J. R. V., Kitchen, J. C., & Pak, H. (1981). The influence of optical water type on the heating rate of a constant depth mixed layer. *Journal of Geophysical Research*, *86*(C7), 6426–6428. https://doi.org/10.1029/JC086iC07p06426

Zhang, R. H., Chen, D., & Wang, G. (2011). Using satellite ocean color data to derive an empirical model for the penetration depth of solar radiation (Hp) in the tropical Pacific Ocean. *Journal of Atmospheric and Oceanic Technology*, *28*(7), 944–965. https://doi.org/10.1175/2011JTECHO797.1

Zoffoli, M. L., Lee, Z., Ondrusek, M., Lin, J., Kovach, C., Wei, J., & Lewis, M. (2017). Estimation of transmittance of solar radiation in the visible domain based on remote sensing: Evaluation of models using in situ data. *Journal of Geophysical Research: Oceans*, *122*, 9176–9188. https://doi.org/10.1002/2017JC013209